**Wind and Structures**, *Vol. 23, No. 5 (2016) 421-447*
DOI: http://dx.doi.org/10.12989/was.2016.23.5.421 

# Numerical simulation of tuned liquid tank- structure systems through σ-transformation based fluid-structure coupled solver

M. Eswaran* and G.R. Reddy

*Structural and Seismic Engineering Section, Reactor Safety Division, Bhabha Atomic Research Centre, Mumbai, 400085, India*

*(Received July 28, 2015, Revised June 30, 2016, Accepted August 10, 2016)*

**Abstract.** Wind-induced and earthquake-induced excitations on tall structures can be effectively controlled by Tuned Liquid Damper (TLD). This work presents a numerical simulation procedure to study the performance of tuned liquid tank- structure system through σ-transformation based fluid-structure coupled solver. For this, a 'C' based computational code is developed. Structural equations are coupled with fluid equations in order to achieve the transfer of sloshing forces to structure for damping. Structural equations are solved by fourth order Runge-Kutta method while fluid equations are solved using finite difference based sigma transformed algorithm. Code is validated with previously published results. The minimum displacement of structure is observed when the resonance condition of the coupled system is satisfied through proper tuning of TLD. Since real-time excitations are random in nature, the performance study of TLD under random excitation is also carried out in which the Bretschneider spectrum is used to generate the random input wave.

**Keywords:** tuned liquid damper; liquid sloshing; transformation; random excitation; computational fluid mechanics

## 1. Introduction

Fluid–structure interaction problems and multi-physics problems in general are often too complex to solve analytically and so they have to be analyzed through experiments or numerical simulation. Research in the fields of computational fluid dynamics (CFD) and computational structural dynamics (CSD) are still ongoing but the maturity of these fields enables numerical simulation of fluid-structure interaction. A fluid-structure interaction phenomenon is an essential consideration in numerous engineering fields. This is distinctly the case in design of offshore structures, long span bridges and high rise buildings, etc. Fluid-structure interaction also plays a vital role in the safety assessment of power generation plants and many other industrial purposes (Jun, Sohn *et al*. 2015). The general topics of fluid-structure interaction is indeed a particularly broad subject in that it simultaneously brings together all the aspects associated with both structural mechanics and fluid mechanics. Each of these two areas are complex by themselves, however, when considered together, the situation becomes even more complex (Donea and Huerta

*Corresponding author, Scientific Officer, E-mail: eswaran@barc.gov.in

**Copyright © 2016 Techno-Press, Ltd.**
http://www.techno-press.org/?journal=was&subpage=8 ISSN: 1226-6116 (Print), 1598-6225 (Online)

2003). In fact, interaction (or coupling) between the fluid and solid response can be viewed as a feedback loop illustrated in Fig. 1 (Eswaran, Saha *et al*. 2009).

If structure heights increases, the flexibility will increase and also the reduced property of inherent damping makes the structure more vulnerable to various forms of external excitations such as earthquakes, varying wind velocities and direction (Eswaran, Verma *et al*. 2016) at great heights, etc. This situation prompted the engineers to implement various types of auxiliary dampers. These absorb major portion of the energy of external excitation and results in damping of the structural vibrations. One such form of auxiliary damper is known as the TLD. A TLD consists of one or more tanks, partially filled with a liquid (usually water), which is typically situated near the top of a building. As the building moves in the severe wind or earthquake attack, the fluid contained within the tank instigates to slosh. Vibrational energy from the structure will be absorbed by fluid and transforms it into kinetic and potential energy of the sloshing fluid. Sloshing forces from damper is used to mitigate the structural responses. Because of its inherent advantages which include easy installation and handling, less maintenance and lower cost, TLDs are progressively being used as vibration absorbers and have fascinated increasing research interest in recent years (Kim *et al*., 2006 *a*, *b*). Practical investigation of such dampers has been reported mainly for controlling wind-induced vibrations in structures (Tamura 1995, Chang 2011). Over the past few years, significant experimental and numerical researches have been done (Modi and Akinturk 2002, Liu, Chiang *et al*. 2003, Jeon, Seo *et al*. 2013) investigated the sloshing fluid of a TLD equipped with damping screens.

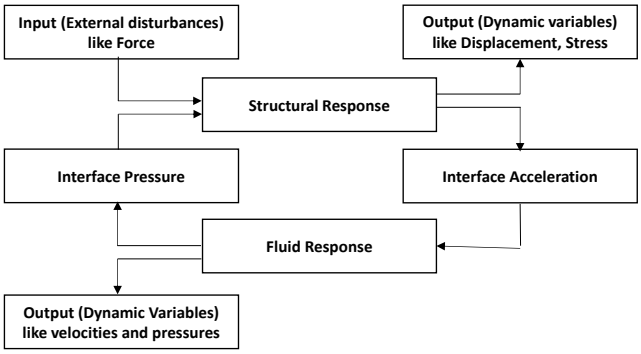


Fig. 1 Feedback loop in fluid structure interaction (Eswaran, Saha *et al*. 2009)

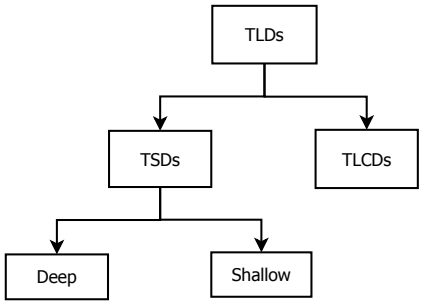


Fig. 2 Classification of TLD (Kareem 1999)

Sloshing is referred to as the oscillation of the free surface of the liquid in a partially filled container due to external excitation (Liu and Lin 2008, Eswaran, Virk *et al*. 2013). These excitations can generate severe hydrodynamic loads and cause stability issues in vessels, vehicles, etc. When the oscillation frequency of the fluid coincides with the first mode natural frequency of the tank, then resonance will occur. Naturally, the accurate tracking of time-varying free surface configuration becomes a significant task for the reliable prediction of the sloshing time-history response (Cho and Lee 2005). Hence, a behavioral study of accurate liquid free surface is necessary for the design of liquid containers which can be subjected to different types of excitation. This can be considered as the negative impact of sloshing which have urged the civil engineers and seismologists to study and analyze its effects on large dams, oil tanks and elevated water towers under ground motion (Eswaran, Virk *et al*. 2013, Eswaran and Reddy 2015 and Eswaran and Reddy 2016). Similarly, the positive effects of sloshing can also be taken into consideration in which case the force of sloshing be transferred effectively.

### *1.1 Tuned liquid damper*

The TLDs have been incorporated in various structures around the world, mostly in Japan (Kareem 1999). As reported by Corbi (2006), 80 TSD units were installed in the 105 m Hobart Tower in Tasmania, Australia. The top floor of the 158 m Gold Tower in Kagawa, Japan, is equipped with 16 units of TSD which helped in the reduction of the response to 50% to 33% of the original response. An alternative multi-layer configuration of the TSD was installed in the 42 m Nagasaki Airport Tower in 1987, and also in the 149 m Shin Yokohama Prince Hotel, Yokohoma in Japan in 1991. Other Japanese implementations include the 1400 vessels installed in the 77.6 m Tokyo International Airport Tower at Haneda, 8 TSD units in the Shanghai World Financial Centre, etc. One Rincon Hill San Francisco, California (Fig. 3) has a large tuned sloshing damper which holds up to 50,000 gallons of water and weighs 416,500 pounds at the top of the building (Nolte 2007).

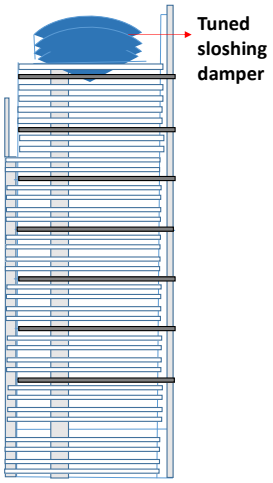


Fig. 3 TSD unit in One Rincon Hill, San Francisco, California (Imprecise sketch and not to scale )

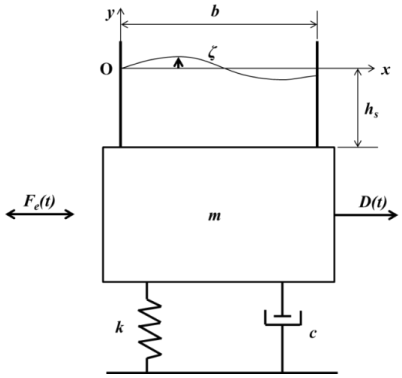


Fig. 4 Schematic of the coupled system

Tuned Liquid Dampers (TLDs) are referred to as the motion activated passive systems or dampers which do not require an external power source in order to effect the dissipation of the structural vibration energy. These are generally tuned to operate at the resonant frequency of the structure but rather in out-of-phase so as to mitigate the structural response. TLDs can be generally classified into two main forms based on their application, namely Tuned Sloshing Dampers (TSDs) and Tuned Liquid Column Dampers (TLCDs). The TSDs is further sub-divided into the deep water and shallow water configurations based on the level of water maintained in the container. The classification is illustrated in Fig. 2. The working principle of a TLD is based on the force of liquid sloshing to absorb a portion of dynamic energy of structure subjected to seismic excitation and thus resulting in damping of structural vibration (Bhattacharjee 2013). The sloshing forces are in opposite direction when compared to that of excitation force thereby inducing the damping effect. Large wave amplitudes can be expected when the structure is excited at a frequency near to the natural frequency of the TLD. At the resonance condition of the TLD-structure system, that is, when the structure is tuned to vibrate at the fundamental frequency of the TLD, significant amount of energy is released. The dissipation of energy in the shallow water TSD is mainly through viscous action and wave breaking while the deep water configuration requires components such as baffles or screens in order to dissipate the sloshing energy efficiently (Kareem 1999). Tuned Liquid Column Dampers (TLCDs) work on the combination of two major effects, which are, the effect of liquid motion in any arbitrary shaped tube which causes a restoring force because of gravity effect, and the damping effect due to loss of hydraulic pressure. The TLCDs have several advantages such as low cost, ease of installation and maintenance requirements, non-restriction to unidirectional excitations, also act as a reservoir of water at the top of buildings for fire suppression, etc. (Balendra 2001).

### *1.2 σ-transformation*

In the discretization methods adopted to solve the free surface governing equations, it is required to incorporate an additional smoothing in order to overcome the instabilities associated with propagation of errors along the boundary (Chern, Borthwick *et al*. 1999). The σ-transformation technique is used to capture the time-varying liquid free surface and map onto a

fixed rectangular domain or a plane surface by proper coordinate transformations (Eswaran, Virk *et al*. 2013, Frandsen 2005). This helps in converting the moving free surface in the physical plane to a fixed line in the computational mapped domain. This technique is illustrated in following chapters in detail. The major advantages are that remeshing due to moving free surface is not required and the free surface velocity components are not explicitly needed as part of the computation process (Frandsen 2005, Frandsen and Borthwick 2003). Frandsen (2005) developed a fully non-linear 2-D σ-transformed finite difference solver to study the behaviour of tuned liquid tank structural systems under regular excitation.

### *1.3 Problem definition*

In order to find the displacement in TLD coupled structure, many literatures are calculating the liquid forces through spring- mass model. These equations and derivations for simple geometries like rectangular and cylindrical tanks can be found in ACI (2006), Housner (1963) and Dodge (2000). This spring mass model is not considering the non-linear motion of the wave. The response of a tuned liquid damper, even for small amplitude motions, is highly non-linear due to liquid sloshing. Therefore, it is necessary to do fluid-structure coupled analysis for the accurate predictions of the structural motions. This study focuses on the analysis of behaviour of TLDs through numerically coupled fluid- structure interaction model for the accurate predictions.

### *1.4 Objective*

The main objective is to analyze the effectiveness of a TLD in reducing the structural vibrations which is externally excited and also to study the impact of various parameters such as frequency ratio, tuning ratio and forcing factor on the damping action of the TLD under regular excitation through fluid-structure coupled solver. Since the real time excitations are random in nature, it is necessary to investigate the effectiveness of the TLD under random excitation by incorporating a well-known spectrum to generate the random input wave.

## 2. Numerical methodology

The coupled interaction between a horizontally excited structure and non-linear motion of liquid in a 2-D rectangular tank is studied. The schematic of such a coupled system is shown in Fig. 4 The rectangular tank is of length b and has a still water depth of $h_s$. In order to effect the purpose of coupling, it is attached to a rigid structure of mass m, damping c and stiffness k. A rectangular Cartesian coordinate system with origin at the mean free-surface at the left wall of the tank is initially employed. From Fig.4, the free surface elevation above the still water level is denoted by $\zeta$. An external horizontally excited force $F_e(t)$ is applied to the system and the motion of the coupled system is denoted by $D(t)$. Taking into assumption that the fluid in the tank is inviscid, irrotational and is governed by potential flow theory, the velocity potential $\phi$ satisfies the Laplace equation.

The non-dimensional parameters are given by $\zeta = A_d \bar{\zeta}$ , $d = A_d D$, $\phi = A_d (h_s g)^{1/2} \bar{\phi}$ and $t = \tau / \omega$ where $A_d = f_f \times h_s$. Here, $\bar{\zeta}$ , $D$ , $\tau$ and $\bar{\phi}$ denote non-dimensional slosh height, structural

displacement, time and velocity potential respectively. The non-dimensional structural properties of mass, stiffness and damping are obtained as $m = \bar{m}/\rho h_s^2$, $k = \bar{k}/\rho g h_s$ and $c = \bar{c}/\rho h_s\sqrt{g h_s}$. The different parameters employed are tuning ratio, $\Omega_t = \omega_1/\omega_0$, where $\omega_1$ is the first mode sloshing frequency, $\omega_n = \sqrt{gk\tanh(k_n h_s)}$, where $k_n = n\pi/b$ and $\omega_0$ is the first natural structural frequency; frequency ratio, $\beta = \omega/\omega_0$, where $\omega$ is the excitation frequency; mass ratio, $M_r = \rho b h_s/\bar{m}$, is the ratio of fluid mass to structural mass; and forcing factor, $f_f = Amp/\rho g h_s^2$, where Amp is the external force characteristic amplitude. Non-dimensional total mass implies, $M_t = m + b h_s$.

### 2.1 Mathematical formulation for fluid and structure

The governing equation and the boundary conditions in the (*x*,*y*,*t*) coordinate system in non-dimensional form are formulated as

$$\text{governing equation,} \qquad \frac{\partial^2\bar{\phi}}{\partial x^2} + \frac{\partial^2\bar{\phi}}{\partial y^2} = 0 \tag{1}$$

$$\text{and boundary conditions,} \quad \frac{\partial\bar{\phi}}{\partial x} = 0; \quad \text{at} \quad x = 0,\ b \quad \text{(left and right walls)} \tag{2}$$

$$\frac{\partial\bar{\phi}}{\partial y} = 0; \quad \text{at} \quad y = -h_s \quad \text{(bottom wall)} \tag{3}$$

The kinematic and dynamic boundary conditions at the free-surface are given by as respectively

$$\frac{\partial\bar{\zeta}}{\partial t} = \frac{\partial\bar{\phi}}{\partial y} - f_f\frac{\partial\bar{\phi}}{\partial x}\frac{\partial\bar{\zeta}}{\partial x} \tag{4}$$

$$\frac{\partial\bar{\phi}}{\partial t} = -\left[\bar{\zeta} + xD''(t) + f_f\frac{1}{2}\left(\nabla\bar{\phi}\right)^2\right] \tag{5}$$

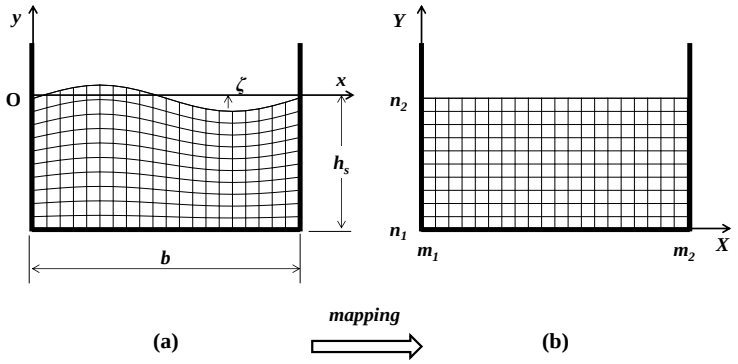


(a) Physical domain (b) Computational domain

Fig. 5 Mapping of liquid

The external excitation induces motion to the structure which generates the horizontal acceleration of the tank $D''(t)$ and is obtained from the equation of motion of the coupled system

$$mD''(t) + cD'(t) + kD(t) = \bar{F}_e(t) + \bar{F}_i(t) \tag{6}$$

where, $F_i(t)$ is the internal force component which is applied to the structure by the sloshing action of the water in the tank. The non-dimensional $\bar{F}_i(t)$ is obtained by $F_i(t)/Amp$, where $F_i(t)$ denotes the dimensional form. This component can be obtained by integrating the pressure values over the right and left tank walls.

$$F_i(t) = \int_{-h_s}^{\zeta} p(x, y, t)dy; \quad \text{over } x = 0 \text{ and } b. \tag{7}$$

where, pressure p is obtained from the unsteady Bernoulli equation

$$\frac{p}{\rho} = -\frac{\partial \phi}{\partial t} - gy - xD''(t) - \frac{1}{2}(\nabla \phi)^2 \tag{8}$$

The initial conditions are such that the structure is assumed to be at rest and the water surface is still and undisturbed.

$$\bar{\phi}(t=0) = 0; \quad \bar{\zeta}(t=0) = 0; \quad D''(0) = F_e(0)/m; \quad D(0) = 0 \quad \text{and} \quad D'(0) = 0 \tag{9}$$

The acceleration condition contains only the term of external force since the contribution of the internal force is zero when the fluid is at rest). Now, as discussed in section 1.2, the σ-transformation technique is used to map onto a fixed rectangular domain or a plane surface by proper coordinate transformations. More details can be found about mapping in Eswaran, Virk *et al*. (2013).

### *2.2 Transformation and discretization*

Fig. 5 illustrates the mapping of (*x,y,t*) coordinate domain to the (*X,Y,T*) coordinate domain and the transformation is referred to as the σ-transformation technique. According to Frandsen and Borthwick (2003), the advantages of introducing the technique are that remeshing due to the moving free surface and the need for calculating the free surface velocity components explicitly are avoided. The mappings from the physical domain *(x,y,t)* to computational domain *(X,Y,T)* are as follows

$$X = m_1 + \frac{(m_2 - m_1)}{b}x \quad \text{and} \quad Y = n_1 + \frac{(n_2 - n_1)(y + h_s)}{h} \tag{10}$$

where $h = \bar{\zeta} + h_s$. The initial transformation of the velocity potential $\bar{\phi}$ are formulated as follows

$$\frac{\partial \bar{\phi}}{\partial x} = \frac{(m_2 - m_1)}{b}\left(\frac{\partial \Phi}{\partial X} + \frac{\mathrm{M}}{h}\frac{\partial \Phi}{\partial Y}\right) \tag{11}$$

$$\frac{\partial \bar{\phi}}{\partial y} = \frac{(n_2 - n_1)}{h}\left(\frac{\partial \Phi}{\partial Y}\right) \tag{12}$$

$$\frac{\partial \bar{\phi}}{\partial t} = \left( \frac{\partial \Phi}{\partial T} + \frac{\mathrm{N}}{h} \frac{\partial \Phi}{\partial Y} \right) \tag{13}$$

where $\mathrm{M} = -(Y - n_1)\left( \frac{\partial \bar{\zeta}}{\partial X} \right)$ and $\mathrm{N} = -(Y - n_1)\left( \frac{\partial \bar{\zeta}}{\partial T} \right)$. Hence, the governing Laplace equation can be obtained as

$$\frac{\partial^2 \Phi}{\partial X^2} + \frac{1}{h}\left[ \frac{\partial \mathrm{M}}{\partial X} - \frac{2\mathrm{M}}{h} \frac{\partial h}{\partial X} \right] \frac{\partial \Phi}{\partial Y} + 2\frac{\mathrm{M}}{h} \frac{\partial^2 \Phi}{\partial Y \partial X} + \left[ \frac{\mathrm{M}^2}{h^2} + \frac{b^2 (n_2 - n_1)^2}{h^2 (m_2 - m_1)^2} \right] \frac{\partial^2 \Phi}{\partial Y^2} = 0 \tag{14}$$

The boundary conditions on the left and the right tank walls at $m_1$ and $m_2$ coordinates and on the bottom wall at $n_1$ coordinate of the computational domain are calculated as

$$\frac{\partial \Phi}{\partial X} = -\frac{\mathrm{M}}{h} \frac{\partial \Phi}{\partial Y} \tag{15}$$

$$\frac{(n_2 - n_1)}{h} \left( \frac{\partial \Phi}{\partial Y} \right) = 0 \tag{16}$$

The transformed kinematic and dynamic free surface boundary conditions at $n_2$ coordinate of the computational domain can be formulated respectively as

$$\frac{\partial \bar{\zeta}}{\partial T} = \frac{(n_2 - n_1)}{h} \frac{\partial \Phi}{\partial Y} \left[ 1 + \frac{(m_2 - m_1)^2}{b^2} \left( \frac{\partial \bar{\zeta}}{\partial X} \right)^2 - \frac{(m_2 - m_1)^2}{b^2} \frac{\partial \bar{\zeta}}{\partial X} \frac{\partial \Phi}{\partial X} \right] \tag{17}$$

$$\frac{\partial \Phi}{\partial T} = \frac{(n_2 - n_1)}{h} \frac{\partial \Phi}{\partial Y} \frac{\partial \bar{\zeta}}{\partial T} - \frac{1}{2}\left[ \frac{(m_2 - m_1)^2}{b^2} \left( \frac{\partial \Phi}{\partial X} - \frac{(n_2 - n_1)}{h} \frac{\partial \Phi}{\partial Y} \frac{\partial \bar{\zeta}}{\partial X} \right)^2 + \frac{(n_2 - n_1)^2}{h^2} \left( \frac{\partial \Phi}{\partial Y} \right)^2 \right] - g\bar{\zeta} - \left( \frac{X - m_1}{m_2 - m_1} \right) bD''(T) \tag{18}$$

The term,

$$D''(t) = \left( \frac{1}{m + \rho b h} \right) \left[ \bar{F}_e(T) + \bar{F}_i(T) - cD'(T) - kD(T) \right] \tag{19}$$

defines the horizontal acceleration of tank generated by the motion of the structure. The internal force developed due to the action of liquid sloshing is given by

$$\bar{F}_i(T) = B_{SF} + P_F; \quad \text{where} \tag{20}$$

$$B_{SF} = \frac{1}{2} \rho g \left( \bar{\zeta}(0,T)^2 - \bar{\zeta}(b,T)^2 \right) \tag{21}$$

$$P_F = \rho \int_{Y=n_1}^{Y=n_2} \left[ \frac{\partial \Phi}{\partial T} + \frac{\mathrm{N}}{h} \frac{\partial \Phi}{\partial Y} + \frac{1}{2}\left( \frac{(m_2 - m_1)}{b} \left( \frac{\partial \Phi}{\partial X} + \frac{\mathrm{M}}{h} \right) \right)^2 + \frac{1}{2}\left( \frac{(n_2 - n_1)}{h} \left( \frac{\partial \Phi}{\partial Y} \right) \right)^2 \right] \frac{h}{n_2 - n_1} dY \tag{22}$$

method by giving the necessary inputs of fluid mass and the structural mass, damping and stiffness along with the displacement and velocity components. In the current study, a finite difference scheme is used for the numerical study of the liquid sloshing. The governing equation and boundary conditions in the computational domain are discretized using finite difference method. Adams-Bashforth scheme is utilized for the computation of nonlinear solutions. As Adams-Bashforth scheme requires results from previous time steps to calculate the current time

step result, hence the semi-implicit scheme is used to generate results for the initial time steps. Pre-conditioned Bi-Conjugate gradient with stabilization (PBiCGSTAB) is used as iterative solver. De (2014) has found the rate of convergence improves significantly from the Strongly Implicit Procedure (SIP) method to the PBiCGSTAB technique while Bi-Conjugate gradient with stabilization (BiCGSTAB) lies between them with non-monotonic convergence. Hence, it is essential for the iteration to have proper evaluation of error to ensure the accuracy of solutions. Error estimation technique is adopted for estimate the error in iterations (Eswaran, Virk *et al*. 2013). The PBiCGSTAB is produces pretty accurate results. Error estimation procedure is better than the difference procedure used to stop the iterative solver, since the difference between two successive iterations falling below a particular limit does not ensure that the iteration error has also fallen down by the same order. The errors for all the cases studied were found to be within the range of $10^{-12}$.

Table 1 Case studies and test parameters with $h$ =1$m$, $b/h$=2, $M_r$ =1%.

| Sl. No. | TLD | $\beta$ | $\Omega_t$ | $f_f$ | $\xi$ | $M_t$ | $k$ | $c$ |
|---|---|---|---|---|---|---|---|---|
| 1 | No TLD | 1 | 1 | 1.0E-04 | 0.0013 | 202 | 291.01 | 0.63 |
| 2 | With TLD | 1 | | | | | | |
| 3 | | 0.6 | | | | | | |
| 4 | | 0.8 | | | | | | |
| 5 | | 0.974 | | | | | | |
| 6 | | 1 | | | | | | |
| 7 | | 1.04 | 1 | | | | 291.01 | 0.63 |
| 8 | | 1.2 | | | | | | |
| 9 | | 0.974 | 0.3 | 1.0E-04 | 0.0013 | 202 | 3233.4 | 2.10 |
| 10 | | 0.974 | 0.6 | | | | 808.37 | 1.05 |
| 11 | | 0.974 | 0.974 | | | | 306.75 | 0.647 |
| 12 | | 0.974 | 0.99 | | | | 296.92 | 0.64 |
| 13 | | 0.974 | 1.2 | | | | 202.09 | 0.53 |
| 14 | | 0.974 | 1 | 0.1 | | | 291.01 | 0.63 |
| 15 | | 0.974 | 1 | 1.0E-04 | 0.0013 | 404 | 208.08 | 0.75 |
| 16 | | | | | | 606 | 152.45 | 0.79 |
| 17 | NO TLD | - | 1 | 1.0E-04 | 0.0013 | 202 | 291.01 | 0.63 |
| 18 | With TLD | - | | | | | | |

## 3. Results and discussion

### 3.1 Grid independence and validation

The grid independence study is carried out for various grid sizes of $41 \times 41$, $61 \times 61$, $81 \times 81$ and $101 \times 101$, for two different non-dimensional time steps of 180 and 190, under the conditions of near resonance at $\beta = 0.974, \Omega_t = 1, M_r = 0.01$ *and* $f_f = 0.0001$, for the first sloshing mode ($n$=1). The different case studies performed and other parameters adopted for the test series are given in Table 1.

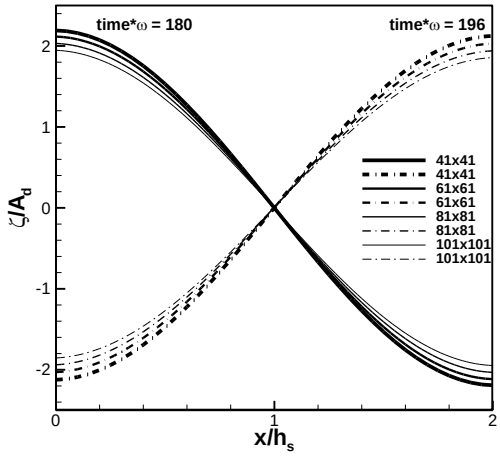


Fig. 6 Grid independence plot

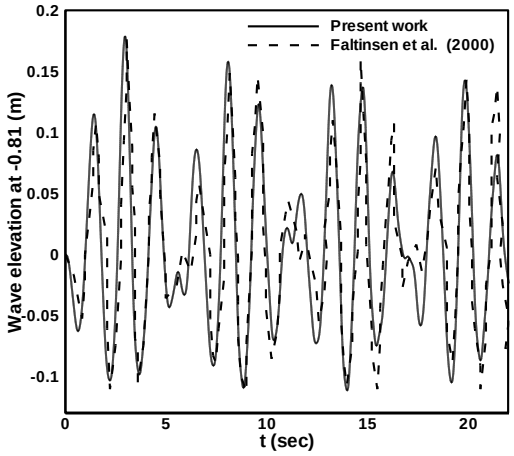


Fig. 7 Code validation with solution of Faltinsen, Rognebakke *et al*. (2000) for free-surface elevation at the left wall in horizontally excited container; $\omega_h$ = 1.283; $A_h$ = 0.029 *m* and $K_h$ = 0.069

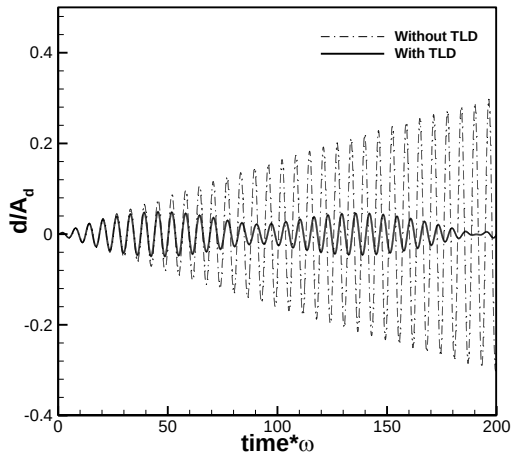


Fig. 8 Displacement plot with and without TLD

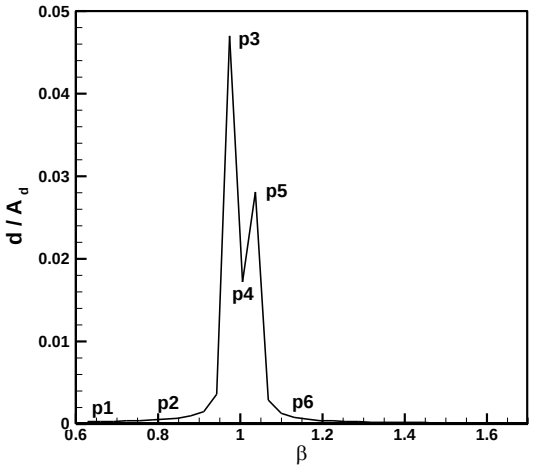


Fig. 9 FFT plot of displacement curve with TLD

The result is illustrated in the Fig.6 in which the non-dimensional free surface elevation is plotted against the length of the tank. As depicted from Fig. 6, the maximum slosh height is found to be in a decreasing trend from the grid size of $41 \times 41$ and finally converges at grid size of $101 \times 101$. Since there is no drastic variation between the values from grid sizes of $81 \times 81$ and $101 \times 101$, the latter grid resolution is taken for the analysis of case studies. Faltinsen, Rognebakke *et al*. (2000), Faltinsen (1974), and Faltinsen and Timokha (2002) did comprehensive analysis of sloshing through theoretical and experimental techniques to provide results considered as benchmark results for the sloshing problems. Fig. 7 shows the comparison of present numerical work with theoretical result of Faltinsen, Rognebakke *et al*. (2000) for the test case: $\omega_h = 1.283$; $A_h$

= 0.029 *m* and $K_h$ = 0.069. The wave peaks and troughs match well with present work. Therefore, the numerical solution was in reasonable agreement with the work of Faltinsen, Rognebakke *et al.* (2000) for this particular test case. The specific test case was previously solved by Hill (2003) and Frandsen (2004) and similar results were obtained.

The forced harmonic motion for various case studies is denoted by, $F_e(t) = Amp.\cos(\omega t)$, where $\omega$ is the excitation angular frequency. A case study for with and without TLD denoted by case 1 and 2, is conducted to analyse the effect of the application of TLD with $\beta = 1,\ \Omega_t = 1,\ M_r = 0.01\ and\ f_f = 0.0001,$ and the non-dimensional displacement plotted against non-dimensional time is shown in Fig. 8. It is clearly seen that the structural displacement is greatly reduced with the application of TLD when it is tuned to the structural natural frequency. FFT analysis is performed on the case and two dominant frequencies are observed as shown in Fig. 9. For this case, the dominant frequencies are obtained at frequency ratio 0.974 and 1.04. Similar results were obtained by Frandsen (2005) through his analytical derivations. The conditions at P3 and P5 are more dissipating energy than other points as these two points are representing the dominant frequencies. So, more structure vibration and subsequently more energy dissipation can be seen at these points than P4. The case studies to analyse the effect of frequency ratio (Sec. 3.2) is performed based on the selected frequency ratios as shown in Table 2. In this work, TLD is tuned to structural first mode natural frequency. Frequency ratio is taken at 6 locations (points) around frequency ratio one for further investigation as shown in Fig. 16 and Table 2.

Figs. 10 and 11 illustrate the plots of non-dimensional displacement and slosh height against non-dimensional time respectively with $\beta = 0.974, \Omega_t = 1, M_r = 0.01$ and $f_f = 0.0001,$ since point p3 is observed as the dominant value. The curvature of the plot of displacement when compared to that of Fig.8 is considered to be the effect of inclusion of the sloshing forces that damp the vibration. Fig.12 illustrates the plot of non-dimensional slosh height with non-dimensional time across the length of the tank. It clearly indicates that the amplitude of wave profile keeps on increasing with time under sinusoidal excitation.

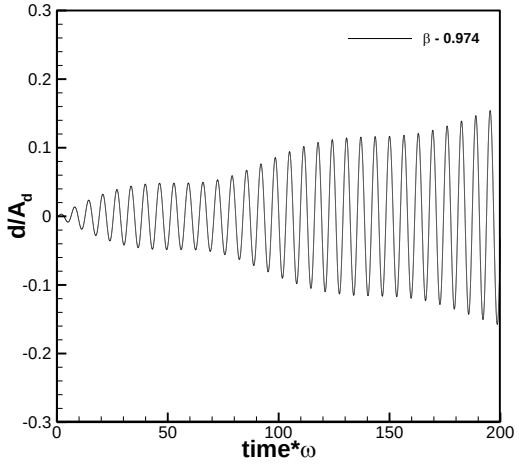


Fig. 10 Displacement plot at β=0.974

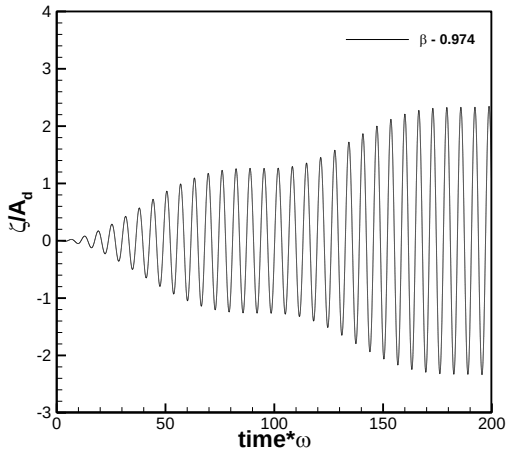


Fig. 11 Slosh height plot at β=0.974

Table 2 Adopted frequency ratio

| Points | p1 | p2 | p3 | p4 | p5 | p6 |
|---|---|---|---|---|---|---|
| $\beta = \omega / \omega_0$ | 0.6 | 0.8 | 0.974 | 1.0 | 1.04 | 1.2 |

### *3.2 Effect of frequency ratio ( $\beta$ )*

This case study features the effect of frequency ratio with $\Omega_t = 1$, $M_r = 0.01$ and $f_f = 0.0001$, as fixed parameters represented by cases 3 to 8. Fig. 12 shows the plot of non-dimensional displacement against non-dimensional time under different frequency ratio. As observed, maximum response is obtained at β = 0.974 and 1.04.

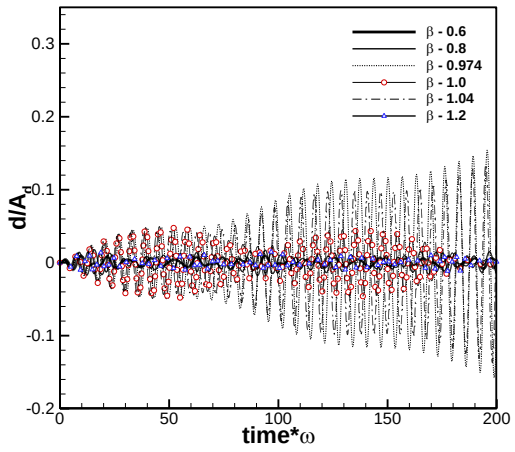


Fig. 12 Displacement plot at different β values

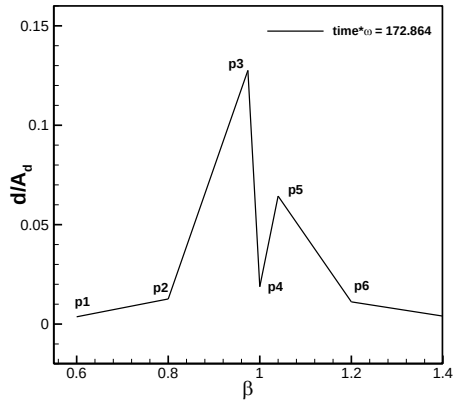


Fig. 13 Displacement amplitude plot with different β values at τ = 172.864

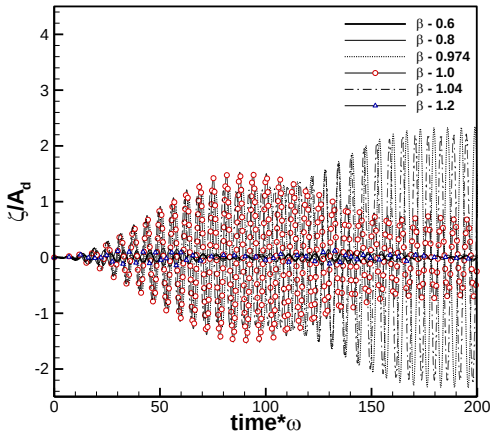


Fig. 14 Slosh height plot at different β values

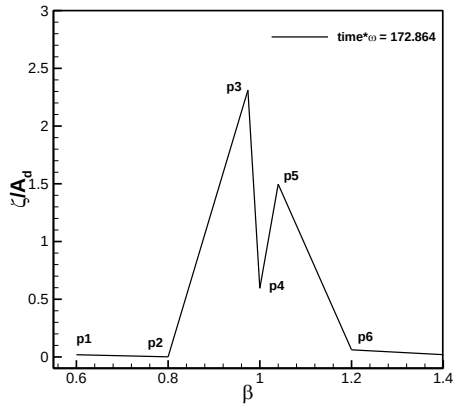


Fig. 15 Slosh height amplitude plot with different β values at τ = 172.864

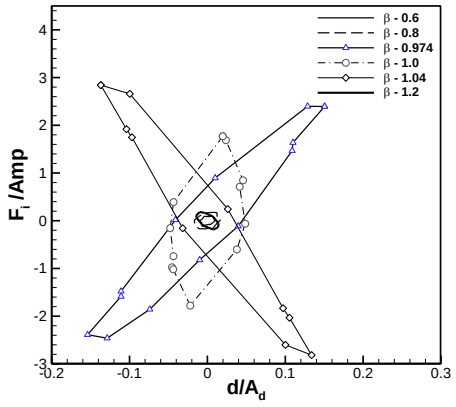


Fig. 16 Energy dissipation plot at different β values

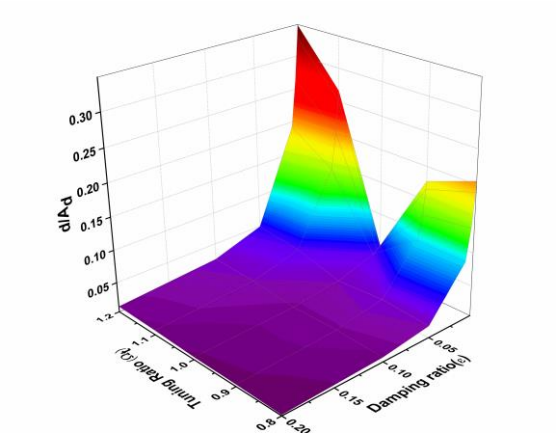


Fig. 17 Non-dimensional displacement with tuning ratio across varying damping ratio

This can be clearly seen in Fig. 13 in which the displacement amplitude is plotted against frequency ratio at non-dimensional time step of 172.864. Similar phenomena can also be observed in the case of plots of non-dimensional slosh height against non-dimensional time and frequency ratio depicted in Figs. 14 and 15 respectively. Minimum response values are observed when the structure is excited with a frequency almost equal to its natural frequency. This situation provides for maximum damping and therefore results in minimal displacement of structure. The energy dissipation curve plotted between non-dimensional internal force and structural displacement is shown in Fig. 16 with different $\beta$ values. It clearly indicates that there is maximum energy dissipated to the structure due to the force of sloshing when the $\beta$ values adopted are near unity. The area of the curves at the above mentioned condition is found to be greater than that of lower $\beta$ values. This energy of sloshing helps in diminishing the displacement and thus results in controlling the structural vibration.

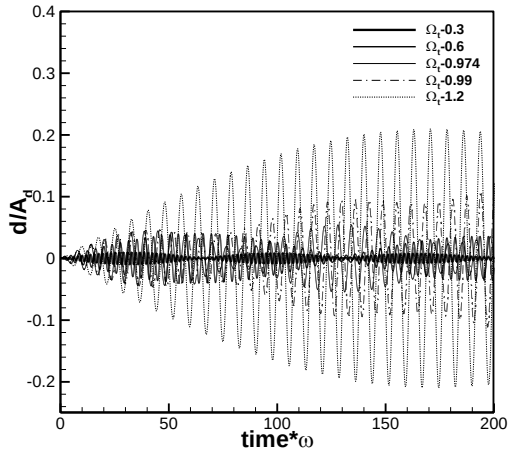


Fig. 18 Displacement plot at different $\Omega_t$ values

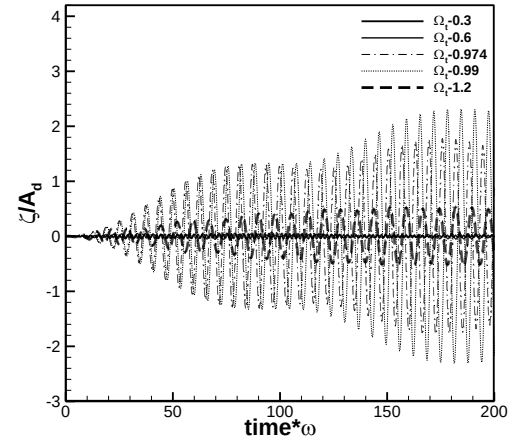


Fig. 19 Slosh height plot at different $\Omega_t$ values

### *3.3 Effect of tuning ratio ($\Omega_t$)*

This case study features the effect of tuning ratio with and $f_f = 0.0001$, as fixed parameters represented by cases 9 to 13. Fig. 17 depicts the plot of variation of non-dimensional displacement at different tuning ratio across varying damping ratio. It is clearly observed that at lower values of damping ratio, the minimum structural response is obtained when the tuning ratio is set as unity. The case study is conducted at $\beta = 1$, in which the structure is excited at its natural frequency. Fig. 17 indicates that as the tuning ratio approaches unity, the maximum structural displacement tends to saturate around a particular value and if it is increased above unity, the maximum displacement seems to be doubled. Non-dimensional displacement and slosh height at different tuning ratio are plotted against non-dimensional time as shown in Figs. 18 and 19 respectively.

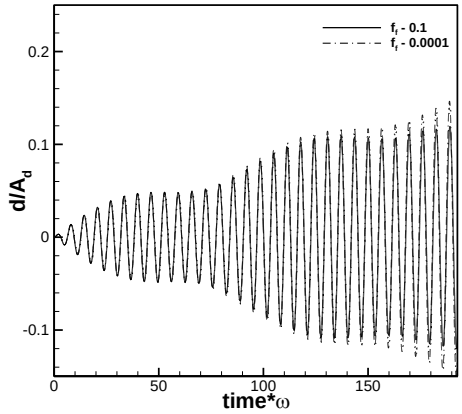


Fig. 20 Displacement plot at different $f_f$ values

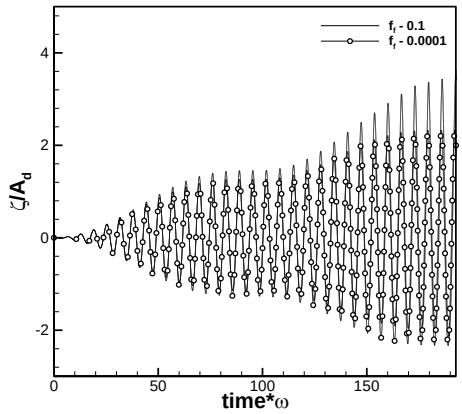


Fig. 21 Slosh height plot at different $f_f$ values

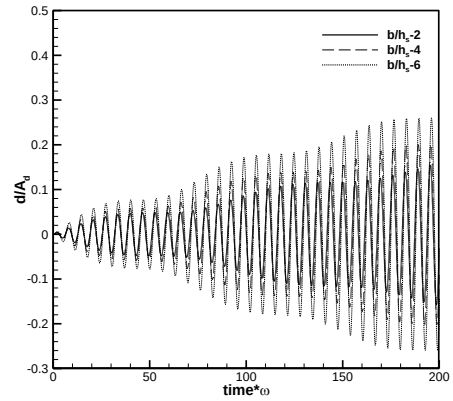


Fig. 22 Displacement plot at different $b/h_s$ ratio

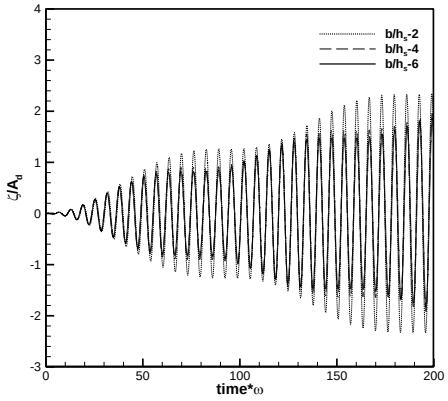


Fig. 23 Slosh height plot at different $b/h_s$ ratio

Fig. 19 illustrates the effect of tuning ratio on slosh height. It is clear that as the tuning ratio approaches unity, the maximum slosh height increases. When the tuning ratio is increased beyond unity, the slosh height is found to decrease drastically. Since greater slosh height is required for maximum internal force thereby increasing the damping effect, the appropriate value to adopt for tuning ratio would be unity.

### *3.4 Effect of forcing factor ( $f_f$ )*

This case study features the effect of forcing factor with $\beta = 0.974$, $M_r = 0.01$ and $\Omega_t = 1$, as fixed parameters represented by case 14. Non-dimensional displacement and slosh height with varying forcing factor are plotted against non-dimensional time as shown in Figs. 20 and 21. it is also observed that as time proceeds, the free surface peaks seem to grow larger when compared to the troughs which are slightly lower.

### *3.5 Effect of aspect ratio ( $b/h_s$ )*

The effect of varying $b/h_s$ ratio is discussed in this section represented by cases 15 and 16. Although the $b/h_s$ ratio is varied, the frequency in the plots of Figs. 22 and 23 remains the same, since it is plotted with non-dimensional displacement and slosh height versus non-dimensional time respectively. The effect is clearly evident from Fig. 22, in which the non-dimensional displacement is plotted against non-dimensional time, in the form of increase in structural displacement as the $b/h_s$ ratio is increased. Therefore the optimum $b/h_s$ ratio to be adopted is 2. It is observed from Fig. 23, in which the non-dimensional slosh height is plotted against non-dimensional time, that there is a decrease and further no significant change in slosh height when the $b/h_s$ ratio is increased and therefore there is insufficient energy produced by the sloshing forces in order to effectively produce the damping action.

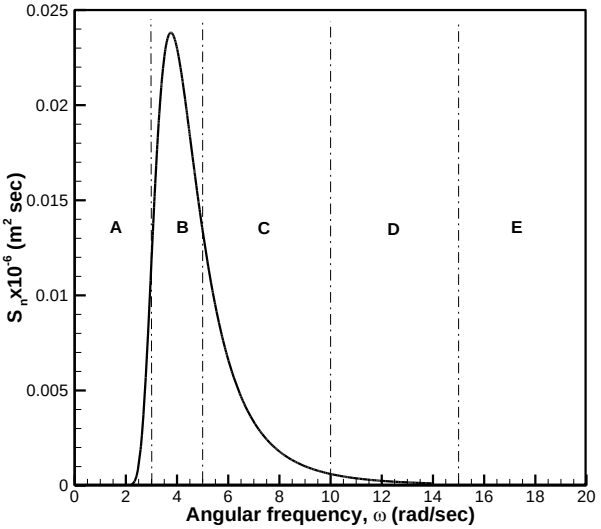


Fig. 24 Bretschneider excitation spectrum with $H_s = 0.001 h_s$ and $\omega_p = \omega_1$.

### *3.6 Random excitation*

Considering most practical situations, the excitation or the variation of time dependent system parameters are random in nature. There are many natural and artificial sources of random excitation. Bretschneider spectrum is selected to serve as the input excitation spectrum for generation of the random input wave. This spectrum is not generally used for structural vibration studies. However, to check the code credibility and vibration control against the random load, the Bretschneider spectrum is used in this work. The relation for the particular spectrum is given in Eq. (22) and is plotted as shown in Fig. 24.

$$S_\zeta(\omega) = \frac{5H_s^{\,2}}{16\omega_p}\left(\frac{\omega_p}{\omega}\right)^5 \exp\left[-\frac{5}{4}\left(\frac{\omega_p}{\omega}\right)^4\right] \tag{22}$$

where $H_s$ is the significant wave height, $\omega_p$ is the peak frequency of the wave. The random input excitation is given by

$$\zeta = \sum_{i=1}^{N_W} A_i \sin\left(\omega^i t + \psi^i\right) \tag{23}$$

where $t$ is time, $\omega^i$ is the frequency of the $i^{th}$ linear wave and $N_W$ is the number of linear monochromatic waves. $\psi^i$ represents the phase of each linear wave and $A_i$ the wave amplitude, which is given by

$$A_i = \sqrt{2S_\zeta(\omega)\Delta\omega} \tag{24}$$

where $\Delta\omega = \omega_{i+1} - \omega_i$, the difference between the adjacent angular frequencies. The number of

linear waves superposed to create the random wave is denoted by $N_W$ and the value of 512 is chosen for the present case. This helps in accommodating lot of frequencies within a given range to contribute towards generation of the random wave. The range of angular frequency is fixed as $\lfloor 0, 5\omega_p \rfloor$ above which the frequencies do not present a significant contribution towards generation of random wave. In this case, $\omega_p$ is taken as the fundamental natural frequency of the system which is 3.7594 *rad/sec*.

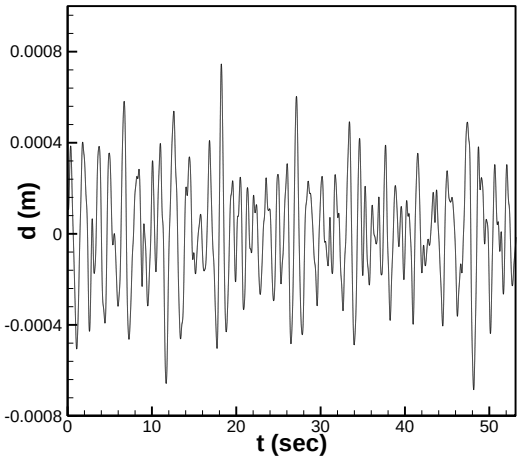


Fig. 25 Displacement generated from spectrum

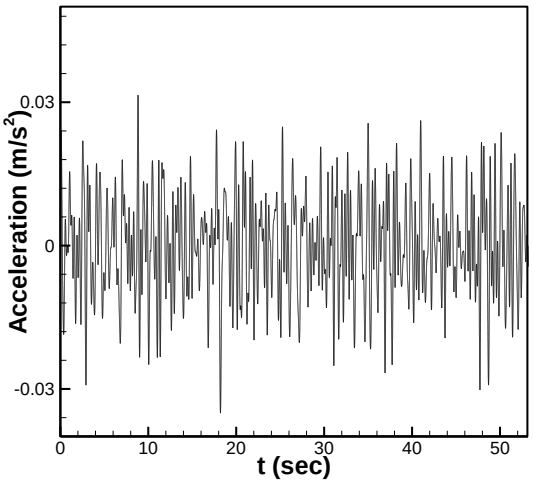


Fig. 26 Acceleration generated from spectrum

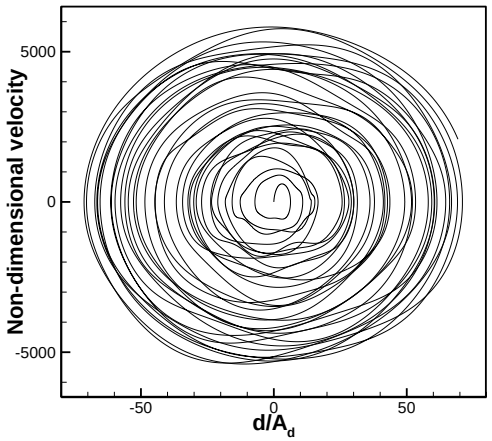


Fig. 27 Phase plane diagram without TLD under random excitation

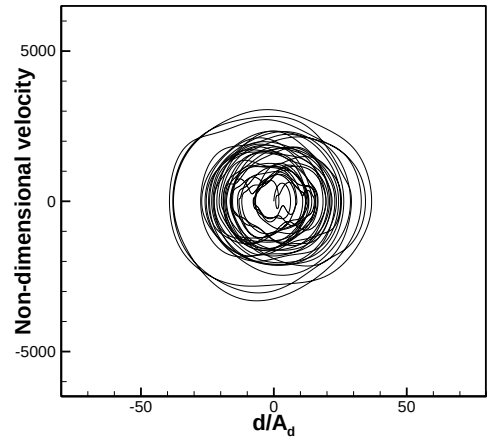


Fig. 28 Phase plane diagram with TLD under random excitation

From Fig. 24, the maximum value of wave energy $(S_\zeta)$ is observed around the peak frequency $(\omega_p)$ and therefore a large number of angular frequencies are chosen in the narrow band around the value of $\omega_p$. As many as 149 values of angular frequencies are selected randomly in the range of $[3.0,5.0]$ which can be observed as a narrow band marked as B. A represents the range $[0.0,3.0]$ and contains 51 values of angular frequencies selected randomly. The regions of C, D and E represent the ranges $[5.0,10.0]$, $[10.0,15.0]$ and $[15.0,5\omega_p]$ and 100 values of angular frequencies are selected randomly respectively. The displacement and acceleration plots generated by the input spectrum are shown in Figs. 25 and 26 respectively. This input displacement values are small than normal scenario. This happens due to the fact that the significant wave height ($H_s$) has been assumed low. As expected, the reduction in structural displacement and velocity is found while

comparing without TLD and with TLD conditions through phase plane diagrams (Figs. 27 and 28). The different peak amplitudes with varying time depict random behaviour. This is also seen in Figs. 27 and 28, which illustrate the phase plane diagrams with and without TLD, with non-dimensional velocity plotted against non-dimensional displacement of structure.

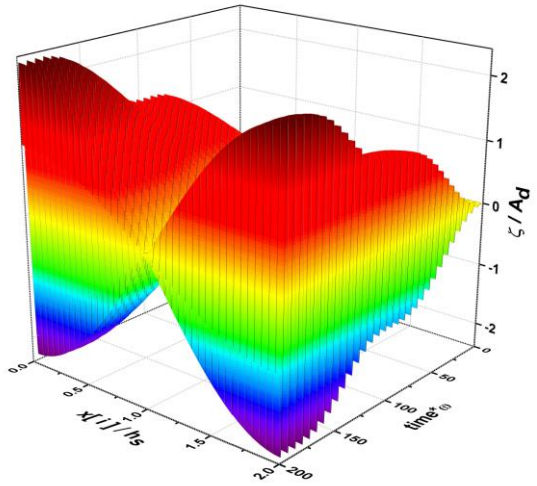


Fig. 29 Variation of slosh height with time across the length of the tank under sinusoidal excitation

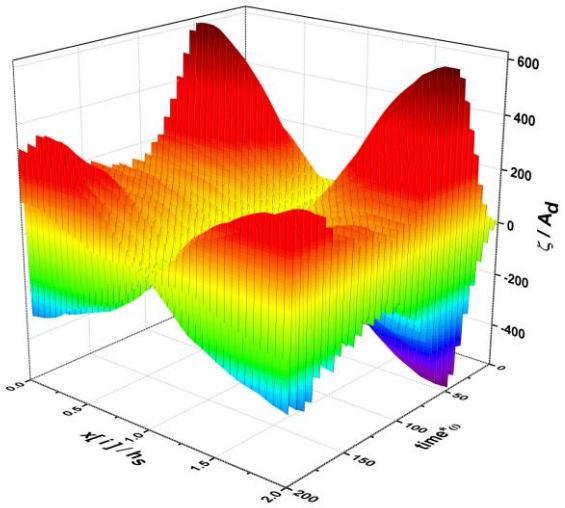


Fig. 30 Variation of slosh height with time across the length of the tank under random excitation

The difference in diametrical values signifies the damping action of the TLD. The plot of non-dimensional slosh height with non-dimensional time across the length of the tank under sinusoidal and random excitation is depicted in Figs. 29 and 30 respectively. The amplitude of

slosh increases rapidly initially, decreases in the same manner and then gradually increases depicting a random behaviour. It is clearly seen that the displacement magnitude is reduced at the resonant frequency thereby mitigating structural response. It is clearly observed that the application of TLD decreases the structural displacement thereby mitigating the structural vibration. Although there is minimum damping during the initial time period, as time proceed the energy developed due to sloshing becomes significant enough such that the forces due to the same are transferred back to the structure and hence the reduction in the amplitude of displacement is observed. A tuned liquid tank-structure system is more effective than structure when excited by sinusoidal load rather than random load. Furthermore, it was found that both frequency ratio and tuning ratio and have significantly affected the response of the Structure-TLD system.

## 4. Conclusions

A numerical study on tuned liquid damper is performed for mitigation of the structural response. With proper tuning of TLD, the displacement of structure is found to be reduced when it is excited at the resonance condition of the coupled system. In this case, the force of liquid sloshing in tank acts as the resisting or damping force to counter the force of excitation. σ-transformation finite difference based technique is employed to solve the fluid boundary conditions and governing equation and capturing the sloshing waves in physical domain and mapping into a rectangular computational domain. The advantages of employing the technique are that remeshing due to moving free surface and the need for explicitly calculating the free surface velocity components are avoided. The structural equations are coupled with fluid equations and the second order structural solver is solved by fourth order Runge-Kutta method. Grid independence studies are carried out initially. The fluid in the tank is assumed to be inviscid, irrotational and governed by potential flow theory. Adams-Bashforth scheme is utilized for computation of non-linear solutions. Force due to liquid sloshing is evaluated and included in the equation of motion of the coupled system which gives the horizontal acceleration of the TLD generated by the motion of the structure. The parametric studies, which included the variation of frequency ratio, tuning ratio, forcing factor and $b/h_s$ ratio, yielded the following results:

i. A case study with frequency ratio, $\beta = 1,$ was conducted with and without the TLD. The structural response was found to be greatly reduced by the addition of TLD. Two distinct frequency ratio values were observed at $\beta = 0.974$ and $\beta = 1.04$ respectively with the inclusion of TLD. The maximum slosh height and displacement values at $\beta = 1.04$ were less than that of $\beta = 0.974$. The slosh height and displacement values were observed to be minimum when excited at the fundamental mode structural frequency.
ii. Tests with varying tuning ratio indicated that as the tuning ratio approached unity, slosh height increases thereby increasing the damping effect. The slosh height decreased drastically when the tuning ratio is increased beyond unity. With greater slosh height, there will be maximum internal sloshing force developed by virtue of which the damping effect can be increased thereby mitigating structural response. Therefore, the appropriate value to be adopted for tuning ratio is unity.
iii. Increasing the forcing factor resulted in a minimum reduction of the structural response when compared to previous cases. As time proceeds, the free surface peaks are observed to grow

larger than the troughs which are slightly lower in amplitude. This results in an imbalance damping effect and hence there is only a slight reduction in structural response.

iv. As the $b/h_s$ ratio is increased, there is an initial decrease in slosh height and further no significant change is observed. This situation leads to insufficient sloshing forces required to produce the damping effect or resist the external excitation force and therefore results in an increased structural displacement. Hence the optimum $b/h_s$ ratio to be taken is 2.

v. A tuned liquid tank-structure system is more effective than structure when excited by sinusoidal load rather than random load. Furthermore, it was found that both frequency ratio and tuning ratio and have significantly affected the response of the Structure-TLD system.

The performance study of TLD under random excitation was also carried out. The particular study was included since in many practical situations, the external excitation is random in nature. Bretschneider spectrum is chosen for the generation of the random input wave. Cases with and without TLD were conducted under random excitation. The amplitude variation in slosh height depicted typical random behaviour and the structural displacement was found to decrease with the application of TLD.

## References

American Concrete Institute Committee 350. (2006), "Seismic design of liquid-containing concrete structures" (ACI 350.3-06) and commentary (350.3R-06), American Concrete Institute, (2006) FarmingtonHills, Mich, USA

Balendra, T., Wang, C.M. and Yan, N. (2001), "Control of wind-excited towers by active tuned liquid column damper", *Eng. Struct.*, **23**, 1054-1067.

Bhattacharjee, E., Halder, L. and Sharma, R.P. (2013), "An experimental study on tuned liquid damper for mitigation of structural response", *Int. J. Adv. Struct. Eng.*, **5**(3), 1-8.

Chang, C.H. (2011), "Computational fluid dynamics simulation for tuned liquid column dampers in horizontal motion", *Wind Struct.*, **14**(5), 435-447.

Chern, M.J., Borthwick, A.G.L, and Taylor, R.E. (1999), "A Pseudospectral σ-transformation model of 2-D nonlinear waves", *J. Fluid. Struct.*, **13**, 607-630.

Cho, J.R. and Lee, H.W. (2005), "Free surface tracking for the accurate time response analysis of nonlinear liquid sloshing", *J. Mech. Sci. Technol.*, **19**(7), 1517-1525

Corbi, O. (2006), "Experimental investigation on sloshing water dampers attached to rigid blocks", *Proceedings of the 5th WSEAS International Conference on Applied Computer Science*, Hangzhou, China.;

De, A.K. (2014), "An implicit non-staggered Cartesian grid method for incompressible viscous flows in complex geometries", *Sadhana*, **39**(5), 1071-1094.

Dodge, F.T. (2000), "The new dynamic behavior of liquids in moving containers", Southwest Research Institute, San Antonio, Texas

Donea, J. and Huerta, A. (2003), "Finite element methods for flow problems", John Wiley & Sons, Ltd., Chichester.

Eswaran, M. and Reddy, G.R. (2015), "Effect of higher modes and multi-directional seismic excitations on power plant liquid storage pools", *Earthq. Struct.*, **8**(3), 779-799.

Eswaran, M. and Reddy, G.R. (2016), "Liquid sloshing in fuel storage bays of advanced reactor subjected to earthquake loading", *Procedia Eng.*, **144**, 1278-1285.

Eswaran, M., Goyal, P., Reddy, G.R., Singh, R.K. and Vaze, K.K. (2013), "Fluid–structure interaction analysis of sloshing in an annular - sectored water pool subject to surge motion", *Ocean Syst. Eng.*, **3**(3), 1-21.

Eswaran, M., Saha, U.K. and Maity, D. (2009), "Effect of baffles on partially filled cubic tank: Numerical simulation and experimental validation", *Comput. Struct.*, **87**(3-4), 198-205.
Eswaran, M., Verma, R.K. and Reddy, G.R. (2016), "Wind-induced loads and integrity assessment of hyperboloid reflector of solar power plants", *Alexandria Eng. J.*, **55**(2), 837-885.
Eswaran, M., Virk, A.S. and Saha, U.K. (2013), "Numerical simulation of 3-D sloshing waves in a regularly and randomly excited container in vertical direction", *J. Marine Sci. Appl.*, **12**(3), 298-314.
Faltinsen, O.M. (1974), "A nonlinear theory of sloshing in rectangular containers", *J. Ship Res.*, **18**(4), 224-241.
Faltinsen, O.M. and Timokha, A.M. (2002), "Asymptotic modal approximation of nonlinear resonant sloshing in a rectangular container with small fluid depth", *J. Fluid Mech.*, **470**, 319-357.
Faltinsen, O.M., Rognebakke, O.F., Lukovsky, I.A. and Timokha, A.N. (2000), "Multidimensional modal analysis of nonlinear sloshing in a rectangular container with finite water depth", *J. Fluid Mech.*, **407**, 201-234.
Frandsen, J.B. (2004), "Sloshing in excited containers", *J. Comput. Phys.*, **196**, 53-87.
Frandsen, J.B. (2005), "Numerical predictions of tuned liquid tank structural systems", *J. Fluid. Struct.*, **20**, 309-329.
Frandsen, J.B. and Borthwick, A.G.L. (2003), "Simulation of sloshing motions in fixed and vertically excited containers using a 2-D inviscid σ-transformed finite difference solver", *J. Fluid. Struct.*, **18**, 197-214.
Hill, D.F. (2003), "Transient and steady-state amplitudes of forced waves in rectangular basins", *Phys. Fluid.*, **15**(6), 1576-1587.
Housner, G.W. (1963), "Dynamic analysis of fluids in containers subjected to acceleration", *Nuclear Reactors and Earthquakes*, Report No. TID 7024, Washington D.C.,USA.
Jeon, S.H., Seo, M.W., Cho, Y.U., Park, W.G. and Jeong, W.B. (2013), "Sloshing characteristics of an annular cylindrical tuned liquid damper for spar-type floating offshore wind turbine", *Struct. Eng. Mech.*, **47** (3), 331-343.
Jun, C., Sohn, J. and Lee, K. (2015), "Dynamic analysis of a floating body in the fluid by using the smoothed particle hydrodynamics", *J. Mech. Sci. Technol.*, **29**(7), 2607-2613.
Kareem, A., Kijewski, T. and Tamura, Y. (1999), "Mitigation of motions of tall buildings with specific examples of recent applications", *Wind Struct.*, **2** (3), 201-251.
Kim, Y.M., You, K.P., Cho, J.E. and Hong, D.P. (2006), "The vibration performance experiment of tuned liquid damper and tuned liquid column damper", *J. Mech. Sci. Technol.*, **20**(6), 795-805.
Kim, Y.M., You, K.P., Ko, N.H. and Yoon, S.W. (2006), "Use of TLD and MTLD for control of wind-induced vibration of tall buildings", *J. Mech. Sci. Technol.*, **20**(9), 1346-1354.
Liu, D. and Lin, P. (2008), "A numerical study of three-dimensional liquid sloshing in tanks", *J. Comput. Phys.*, **227**, 3921-3939.
Liu, M.Y., Chiang, W.L., Chu, C.R. and Shen, S. (2003), Analytical and experimental research on wind – induced vibration in high-rise buildings with tuned liquid column dampers", *Wind Struct.*, **6**(1), 71-90.
Modi, V.J. and Akinturk, A. (2002), "An efficient liquid sloshing damper for control of wind-induced instabilities", *J. Wind Eng. Ind. Aerod.*, **90**(19), 1055-1071.
Nolte, C. (2007), "One Rincon tower features water tank on top to counteract wind", http://www.sfgate.com/bayarea/article/One-Rincon-tower-features-water-tank-on-top-to-3299035.php.
Ross, A.S., Damatty, A.A. and Ansary, A.M. (2015), "Application of tuned liquid dampers in controlling the torsional vibration of high rise buildings", *Wind Struct.*, **21**(5), 537-564.
Tamura, Y. (1995), "Effectiveness of tuned liquid dampers under wind excitations", *Eng. Struct.*, **17**(9), 609-621.

*CC*

## Nomenclature

| | |
|---|---|
| CFD | : Computational Fluid Dynamics |
| TLD | : Tuned Liquid Damper |
| TSD | : Tuned Sloshing Damper |
| TLCD | : Tuned Liquid Column Damper |
| FFT | : Fast Fourier Transform |
| $A_i$ | : Wave amplitude of i$^{th}$ linear wave |
| $A_d$ | : Non-dimensional constant |
| $Amp$ | :External force characteristic amplitude |
| $n$ | : Mode number of oscillation |
| $b$ | : Length of tank |
| $h$ | :Instant water height from tank bottom |
| $h_s$ | : Still water depth |
| $H_s$ | : Significant wave height |
| $N_W$ | : Number of linear monochromatic waves |
| $\rho$ | : Density of water |
| $g$ | : Acceleration due to gravity |
| $\bar{\zeta}$ | :Non-dimensional free surface elevation |
| $\bar{m}, \bar{c}, \bar{k}$ | :Non-dimensional structure mass, damping and stiffness respectively |
| $D$ | :Non-dimensional structural displacement |
| $\tau$ | : Non-dimensional time |
| $\bar{\phi}$ | :Non-dimensional velocity potential function |
| $\bar{F}_e(t)$ | :Non-dimensional external force of excitation |
| $\bar{F}_i(t)$ | : Non-dimensional internal force of sloshing |

$p$ : Pressure

$\omega_n$ :$n^{th}$ mode sloshing angular frequency

$\omega_1$ :First mode sloshing angular frequency

$\omega_0$ : Structural natural frequency

$\omega$ : Excitation angular frequency

$\omega_i$ : Frequency of $i^{th}$ linear wave

$\omega_p$ : Peak frequency of wave spectrum

$k_n$ : Wave number of $n^{th}$ mode

$M_r$ : Mass ratio

$M_t$ : Non-dimensional total mass

$\xi$ : Damping ratio

$f_f$ : Forcing factor

$\Omega_t$ : Tuning ratio

$\beta$ : Frequency ratio

$\phi(x,y,t)$ :Velocity potential function in physical domain $(x,y,t)$

$\Phi(X,Y,T)$: Velocity potential function in computational domain $(X,Y,T)$

$m_1, m_2, n_1, n_2$: Coordinate points on computational domain axes

$S_\zeta$ :Bretschneider spectrum wave energy

$\psi_i$ : Phase angle of $i^{th}$ linear wave

$B_{SF}$ : Base shear force

$P_F$ : Force due pressure at tank walls